

# A cartesian grid finite volume method for the solution of the Poisson equation with variable coefficients and embedded interfaces

M. Oevermann<sup>a,\*</sup> and R. Klein<sup>b,1</sup>

<sup>a</sup>*Technische Universität Berlin, Institut für Energietechnik, Fasanenstr. 89, 10623 Berlin, Germany*

<sup>b</sup>*Freie Universität Berlin, Fachbereich Mathematik und Informatik, Arnimallee 14, 14195 Berlin, Germany*

---

## Abstract

We present a finite volume method for the solution of the two-dimensional Poisson equation  $\nabla \cdot (\beta(\mathbf{x})\nabla u(\mathbf{x})) = f(\mathbf{x})$  with variable, discontinuous coefficients and solution discontinuities on irregular domains. The method uses bilinear ansatz functions on Cartesian grids for the solution  $u(\mathbf{x})$  resulting in a compact nine-point stencil. The resulting linear problem has been solved with a standard multigrid solver. Singularities associated with vanishing partial volumes of intersected grid cells or the dual bilinear ansatz itself are removed by a two-step asymptotic approach. The method achieves second order of accuracy in the  $L^\infty$  and  $L^2$  norm.

*Key words:* Poisson equation, finite volume methods, embedded interface, variable and discontinuous coefficients, discontinuous solution

*1991 MSC:* 35J25, 65N12, 65N30

---

## 1 Introduction

We seek solutions of the two-dimensional variable coefficient Poisson equation

$$\nabla \cdot (\beta(\mathbf{x})\nabla u(\mathbf{x})) = f(\mathbf{x}), \quad \mathbf{x} \in \bar{\Omega} \setminus \Gamma \quad (1)$$

---

\* Corresponding author.

*Email addresses:* michael.oevermann@tu-berlin.de (M. Oevermann), klein@zib.de (R. Klein).

<sup>1</sup> Potsdam Institute for Climate Impact Research Potsdam, Data and Computation, Telegrafenberg C4, 14473 Potsdam, Germany

defined in a domain  $\bar{\Omega} \setminus \Gamma$  with an embedded interface  $\Gamma$ . For simplicity we assume  $\bar{\Omega}$  to be a simple rectangle. The embedded interface  $\Gamma$  separates two disjoint sub-domains  $\bar{\Omega}^+$  and  $\bar{\Omega}^-$  with  $\bar{\Omega} = (\bar{\Omega}^+ \cup \bar{\Omega}^-) \setminus \Gamma$ , see Fig. 1 for an illustration. Along the interface we prescribe jump conditions for the solution

$$[u]_{\Gamma} = u^+(\mathbf{x}) - u^-(\mathbf{x}) = g(\mathbf{x}_{\Gamma}) \quad (2)$$

and for its gradient in the normal direction

$$[\beta u_n]_{\Gamma} = \beta^+ u_n^+ - \beta^- u_n^- = h(\mathbf{x}_{\Gamma}), \quad (3)$$

with the notation  $u_n = (\nabla u \cdot \mathbf{n})$ . The unit normal vector  $\mathbf{n}$  on  $\Gamma$  is defined to point from  $\bar{\Omega}^+$  to  $\bar{\Omega}^-$ .

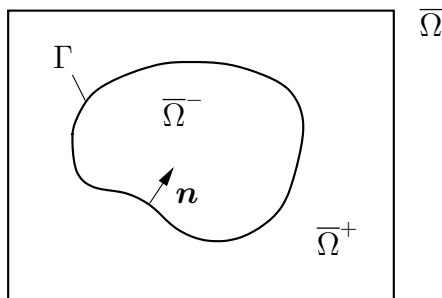


Figure 1. Domain  $\bar{\Omega}$  with sub-domains  $\bar{\Omega}^+$ ,  $\bar{\Omega}^-$ , and embedded interface  $\Gamma$ .

Elliptic equations of type (1) with variable and discontinuous coefficients and solution discontinuities often arise as a component in modelling physical problems with embedded boundaries. Examples include incompressible two-phase flow with surface tension featuring jumps in pressure and pressure gradient across the interface, projection methods for zero Mach-number premixed combustion with jumps in the dynamic pressure and pressure gradient across the flame front, heat conduction between materials of different heat capacity and conductivity and interface diffusion processes. In the literature one can find a number of different approaches for the numerical solution of this type of problem. We limit our discussion here to methods on fixed Cartesian grids.

In Peskin's immersed boundary method [15], singular forces arising from discontinuous coefficients and jump conditions are treated as delta functions. Using discretised discrete delta functions, the discontinuity is spread over several grid cells making the method first order accurate. The method has been used for many problems in mathematical biology and fluid mechanics.

Mayo [12,13] presented a second order accurate method for Poisson's equation and the biharmonic equation on irregular domains using an integral equation formulation. The resulting Fredholm integral equations of the second kind are solved with a fast Poisson solver on a rectangular region. Although the method

captures solution discontinuities at the embedded interface, continuous derivatives have been assumed to evaluate the discrete Laplacian. The method can easily be extended to fourth order accuracy.

The immersed interface method [5,6,7] is a second order finite difference method on Cartesian grids for second order elliptic and parabolic equations with variable coefficients. Discontinuities in the solution and the normal gradient at the interface are explicitly incorporated into the finite difference stencil. Second order has been achieved by including additional points near the interface into the standard 5-point stencil leading to a non-standard six-point stencil in 2D. The resulting linear equation system is sparse but not symmetric or positive definite. Based on the immersed interface method Li and Ito [8] present a second order finite difference method which satisfies the sign property on the matrix coefficients which guarantees the discrete maximum principle. The resulting linear system of equations is non-symmetric but diagonally dominant and its symmetric part is negative definite.

A first order finite difference method on Cartesian grids was presented by Liu et al. [10]. Interface jump conditions are explicitly incorporated into the finite difference stencil as in the immersed interface method. Applying a one-dimensional approach in each spatial direction by implicitly smearing out the gradient jump condition, standard stencils (5-point in 2D, 9-point in 3D) for the discrete Laplacian are achieved leading to a symmetric positive definite matrix for the Poisson equation. The method shows first order accuracy for the solution  $u$  in the  $L^\infty$ -norm for constant coefficients  $\beta^\pm$ . A convergence proof of the method has been provided in [11] based on the weak formulation of the problem.

A finite element method on triangular meshes for solving second order elliptic and parabolic equations for interface problems with  $[u] = 0$  and  $[\beta u_n] \neq 0$  has been proposed by Chen and Zou [1]. In their method the triangles are aligned with the interface. In the  $L^2$ -norm nearly second order accuracy ( $h^2 |\log h|$ ) has been proved. The resulting linear system of equations is symmetric and positive definite. Another finite element method based on uniform triangulations of Cartesian grids was presented by Li et al. [9]. In contrast to [1], the triangles need not be aligned with the interface. Numerical results with non-conforming finite elements demonstrate slightly less than second order of accuracy in  $L^\infty$  and second order of accuracy with conforming finite elements for a problem with homogeneous jump conditions  $[u] = 0$ ,  $[\beta u_n] = 0$ . The general case with variable coefficients and non-homogeneous interface conditions  $[u] \neq 0$ ,  $[\beta u_n] \neq 0$  has been tackled recently by Hou and Liu [3] with a finite element method. Similar to [9] they use uniform triangulations of Cartesian grids. Their method is second order accurate in  $L^\infty$  if the solution  $u$  is  $C^2$  and the interface is  $C^2$  or  $C^1$ .

Johansen and Colella [4] developed a second-order finite volume method on Cartesian grids for the variable coefficient Poisson equation on irregular domains with Dirichlet and Neumann boundary conditions and combined the method with an adaptive mesh refinement. Using central differencing for the gradients, their method reproduces the standard five-point stencil on regular cells. Using linear interpolation of gradients for internal edges and quadratic polynomials in normal direction to the boundary for irregular cells leads to a non-standard stencil. The final linear system is non-symmetric. Although remotely related to our work in the sense of using a finite volume method, the authors did not consider embedded boundaries with jump conditions of the solution and the normal derivative.

In this paper we present a second order finite volume method on Cartesian grids for solving the variable coefficient Poisson equation (1) with embedded interfaces and interface discontinuities. The motivation for a finite volume approach stems from our interest in conservative finite volume projection methods for Zero- and Low-Mach-number flow. The divergence constraint of the velocity field in a natural way leads to a Poisson equation for the pressure in a finite volume form. The use of piecewise bilinear ansatz function for the solution  $u$  makes our method quite similar to finite element methods and allows us to construct improved exact projection methods [17]. In two space dimensions the resulting system of linear equations is assembled from compact 9-point stencils. Compared to the cited literature our method differs in the following points: (i) we use a finite volume method instead of finite difference [5,10] or finite elements [3,9], (ii) compared to the second order immersed interface method [5] we achieve always automatically a compact 9-point stencil without explicit incorporation of additional points near the interface or solution of an optimization problem as in [8], (iii) instead of piecewise linear ansatz-functions on triangles as in the cited finite element methods we use piecewise bilinear ansatz-functions on the Cartesian grid. Compared to the finite element method presented in [3], we are able to construct a bilinear finite element which does not develop singularities when the element degenerates, e.g. vanishing partial volumes of intersected cells. In contrast to the cited finite element methods our methods results in a non-symmetric matrix. In case of constant and equal coefficients we have a symmetric and positive definite matrix. We believe that the presented bilinear element will be useful for other finite element schemes and even for explicit schemes with embedded interfaces and solution discontinuities.

## 2 Finite volume formulation

Integrating equation (1) over an arbitrary control volume  $\Omega \in \bar{\Omega}$  leads to

$$\int_{\Omega} \nabla \cdot (\beta \nabla u) dV = \int_{\Omega} f dV.$$

For a control volume  $\Omega = \Omega^+ \cup \Omega^-$  intersected by the interface we obtain after applying the divergence theorem

$$\int_{\partial\Omega} \beta \nabla u \cdot \mathbf{n} dS = \int_{\Omega} f dV - \int_{\Gamma_{\Omega}} [\beta u_n] dS \quad (4)$$

where  $\Gamma_{\Omega}$  denotes the part of the embedded interface  $\Gamma$  lying inside  $\Omega$  and  $\partial\Omega = (\partial\Omega^+ \cup \partial\Omega^-) \setminus \Gamma_{\Omega}$ . For  $\Gamma_{\Omega} \neq \emptyset$  we have

$$\int_{\Omega} f dV = \int_{\Omega^+} f^+ dV + \int_{\Omega^-} f^- dV. \quad (5)$$

For a regular control volume without an embedded interface we have either  $\Omega = \Omega^+ \in \bar{\Omega}^+ \wedge \Omega^- \equiv \emptyset$  or  $\Omega = \Omega^- \in \bar{\Omega}^- \wedge \Omega^+ \equiv \emptyset$  and the last integral on the right side of (4) vanishes.

## 3 Numerical method

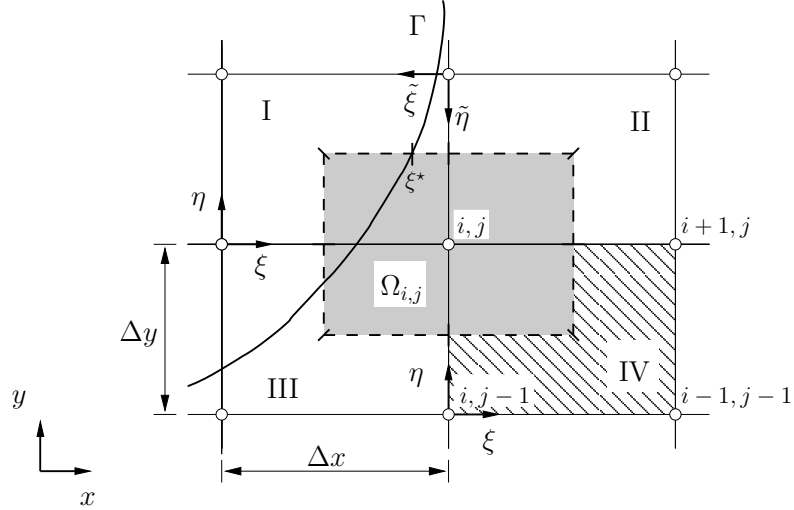


Figure 2. Control volume  $\Omega_{i,j}$ . Discrete solution values are located at the grid nodes marked with circles. Regular cells II, IV, irregular cells I, III.

We discretise (4) on a uniform Cartesian grid in two-dimensional space. Let  $\Delta x$ ,  $\Delta y$  be the grid spacing in x and y-direction, see Fig. 2. The values  $u_{i,j}$  of our discretised solution are located at the grid nodes with the coordinates

$x_{i,j} = x_0 + i \Delta x$ ,  $y_{i,j} = y_0 + j \Delta y$ . The control volumes  $\Omega_{i,j}$  are centered around the corresponding grid nodes  $i, j$  having edges of length  $\Delta x$  and  $\Delta y$ . Let  $\mathfrak{N}_{i,j}$  be the set of rectangles – called cells in this work – adjacent to node  $i, j$  (I – IV in Fig. 2). The discrete form of (4) for the control volume  $\Omega_{i,j}$  now reads as

$$\sum_{N \in \mathfrak{N}_{i,j}} \sum_{i=1}^2 \int_{l_i^N} \beta \nabla u \cdot \mathbf{n} dS = \int_{\Omega_{i,j}} f dV - \int_{\Gamma_{\Omega_{i,j}}} [\beta u_n] dS, \quad (6)$$

where  $l_i^N$ ,  $i = 1, 2$  are the two boundary edges with normals  $\mathbf{n}_1$  and  $\mathbf{n}_2$  of  $\partial\Omega_{i,j}$  lying inside  $N$ .

To evaluate the left hand side of (6) we use a finite element approach with piecewise bilinear ansatz functions for  $u$  on each rectangular cell  $N \in \mathfrak{N}_{i,j}$ .

### 3.1 Bilinear finite elements for regular cells

For any regular cell  $N \in \mathfrak{N}_{i,j}$  without embedded interface we apply a standard bilinear local ansatz

$$u(\xi, \eta) = c_0 + c_1 \xi + c_2 \eta + c_3 \xi \eta, \quad \xi = \frac{x - x_0^N}{\Delta x}, \eta = \frac{y - y_0^N}{\Delta y},$$

with  $\xi, \eta \in [0, 1]$ . Here,  $(x_0^N, y_0^N)$  denotes the origin of the local  $\xi, \eta$ -coordinate system in global  $(x, y)$ -space. The four unknown coefficients are uniquely determined by the four corner values of  $u$ . Given the piecewise bilinear distribution of  $u(\xi, \eta)$  we evaluate the boundary integrals on the left side of (6) analytically. As an example, we have for upper integral of cell IV in Fig. 2

$$\begin{aligned} \int_{l_i^N} \beta \nabla u \cdot \mathbf{n} dS &= \int_{0.5}^1 \beta \frac{\partial u}{\partial \xi} d\eta \\ &= \beta \frac{\Delta y}{\Delta x} \left( \frac{3}{8} (u_{i+1,j} - u_{i,j}) + \frac{1}{8} (u_{i+1,j-1} - u_{i,j-1}) \right) \end{aligned} \quad (7)$$

Integrating over the whole boundary of  $\Omega_{i,j}$  we find in the special case  $\beta = 1$ ,  $\Delta x = \Delta y$  the stencil elements for the discrete Laplacian of a regular control volume as displayed in Fig. 3. This discretization has been analyzed by Süli [16], who proved stability and second order convergence of the scheme on grids with arbitrary aspect ratio  $\Delta x / \Delta y$ .

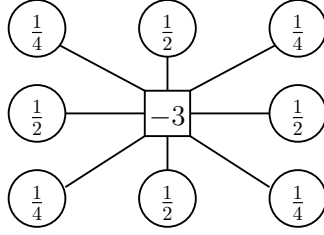


Figure 3. Stencil of the discrete Laplacian for  $\beta = 1$ ,  $\Delta x = \Delta y$

### 3.2 Evaluation of source terms

For a second order approximation of (5) we use

$$\int_{\Omega} f dV = |\Omega^+| f^+(\mathbf{x}_s^+) + |\Omega^-| f^-(\mathbf{x}_s^-), \quad (8)$$

where  $\mathbf{x}_s^{\pm}$  denotes the barycenter of  $\Omega^{\pm}$ .

To avoid additional computations of interface jump conditions, the boundary integral on the right hand side of (6) is evaluated assuming linear distributions of the interface jump conditions within cells. For a second order approximation we have

$$\int_{\Gamma_{\Omega_{i,j}}} [\beta u_n] dS = \sum_{N \in \mathfrak{N}_{i,j}} [\beta u_n] l_{\Gamma_{\Omega_{i,j}^N}}, \quad (9)$$

where  $l_{\Gamma_{\Omega_{i,j}^N}}$  is the part of the interface  $\Gamma_{\Omega_{i,j}}$  in cell  $N$  which belongs to the control volume  $\Omega_{i,j}$ .

### 3.3 Evaluation of the discrete Laplacian on irregular control volumes

In two spatial dimensions on a Cartesian grid, irregular cells can always be mapped onto one of the two unit-square cells shown in Fig. 4 and 6. We call a cell with an interface cutting the two adjacent edges of the upper right corner type I and type II otherwise. The position of the interface is assumed to be a piecewise straight line within the cell and is given by the zero level set of a signed normal distance function  $\phi(\mathbf{x})$ . On each side of the interface we make a bilinear ansatz:

$$\begin{aligned} u^{(\mathfrak{A})}(\xi, \eta) &= a_0 + a_1 \xi + a_2 \eta + a_3 \xi \eta, & \xi, \eta \in \Omega^{\mathfrak{A}}, \\ u^{(\mathfrak{B})}(\tilde{\xi}, \tilde{\eta}) &= b_0 + b_1 \tilde{\xi} + b_2 \tilde{\eta} + b_3 \tilde{\xi} \tilde{\eta}, & \tilde{\xi}, \tilde{\eta} \in \Omega^{\mathfrak{B}}. \end{aligned} \quad (10)$$

The gradients follow immediately

$$\begin{aligned}\frac{\partial u^{(\mathfrak{A})}}{\partial \xi} &= a_1 + a_3 \eta, & \frac{\partial u^{(\mathfrak{A})}}{\partial \eta} &= a_2 + a_3 \xi, \\ \frac{\partial u^{(\mathfrak{B})}}{\partial \tilde{\xi}} &= b_1 + b_3 \tilde{\eta}, & \frac{\partial u^{(\mathfrak{B})}}{\partial \tilde{\eta}} &= b_2 + b_3 \tilde{\xi}.\end{aligned}\quad (11)$$

The procedure of obtaining the eight unknown coefficients

$$\underline{x} = [a_0, a_1, a_2, a_3, b_0, b_1, b_2, b_3]^t \quad (12)$$

is given in detail below. However, we will always be able to write  $\underline{x}$  as a linear combination of the four unknown corner values  $u_i$ ,  $i = 1 \dots 4$  and four known jump conditions  $[u]_A$ ,  $[u]_B$ ,  $[\beta u_n]_A$ , and  $[\beta u_n]_B$ :

$$\underline{x} = \underline{A} \underline{b}, \quad (13)$$

with  $\underline{b} = [\underline{u}^t, [\cdot]^t]^t$ ,  $\underline{u} = [u_1, u_2, u_3, u_4]^t$ , and  $[\cdot]^t = [[u]_A, [u]_B, [\beta u_n]_A, [\beta u_n]_B]^t$ . Furthermore, using (11) we can evaluate any integral on the left hand side of (6) analytically on each irregular (and regular) cell. With (13) we can further express each of these integrals as a linear combination of the four unknown corner values and known jump conditions of the irregular cell. As an example, we consider cell I of the control volume  $\Omega_{i,j}$  in Fig. 2, which is an irregular cell of type II, see Fig. 6. For boundary edge  $l_1^I$  with unit normal  $\mathbf{n} = [n_x, n_y]^t = [0, 1]^t$  we can write

$$\begin{aligned}\int_{l_1^I} \beta \frac{\partial u}{\partial y} dx &= \frac{\Delta x}{\Delta y} \left( \int_{1/2}^{\xi^*} \beta^{(\mathfrak{A})} \frac{\partial u^{(\mathfrak{A})}}{\partial \eta} d\xi + \int_{\tilde{\xi}^*}^0 \beta^{(\mathfrak{B})} \frac{\partial u^{(\mathfrak{B})}}{\partial \tilde{\eta}} d\tilde{\xi} \right) \\ &\stackrel{(11)}{=} \frac{\beta^{(\mathfrak{A})} \Delta x}{\Delta y} \left( a_2 \left( \xi^* - \frac{1}{2} \right) + a_3 \left( \frac{\xi^{*2}}{2} - \frac{1}{8} \right) \right) - \frac{\beta^{(\mathfrak{B})} \Delta x}{\Delta y} \left( b_2 \tilde{\xi}^* + b_3 \frac{\tilde{\xi}^{*2}}{2} \right) \\ &= \underline{D}_1 \underline{u} + \underline{D}_2 [\cdot],\end{aligned}$$

with  $\underline{u} = [u_{i-1,j}, u_{i,j}, u_{i,j+1}, u_{i-1,j+1}]^t$ . Going from the first to the second line we have introduced the gradients given in equation (11) and evaluated the integrals analytically. The matrices  $\underline{D}_1$  and  $\underline{D}_2$  are analytically deduced from  $\underline{A}$  and  $\xi^*$  and they contain only geometric information about the interface within the irregular cell I. Now,  $\underline{D}_1$  determines the stencil coefficients for the discrete Laplacian, whereas  $\underline{D}_2 [\cdot]$  will modify the right hand side of the discretised equation (6). Furthermore, as  $\underline{u}$  only contains the four unknown solution values, we will always obtain a compact nine-point stencil (except for corner or boundary points of  $\bar{\Omega}$ , where we have four or six-point stencils, respectively) during the calculation of the complete boundary integral on the left hand side of (6). We treat the coefficients  $\beta^{(\mathfrak{A})}$  and  $\beta^{(\mathfrak{B})}$  piecewise constant on each cell with values evaluated at the barycenters of the corresponding sub-areas. This procedure is in accordance with [3] and does not seem to effect

the second order of the method. However, it is also possible to evaluate the coefficients either in the midpoint of each integral or to prescribe a distribution and doing the integration again analytically.

### 3.4 Piecewise bilinear finite elements for irregular cells

Using piecewise bilinear ansatz functions (10) on irregular cells, we remark two important properties to get the eight unknown coefficients in  $\underline{x}$ :

**Remark 3.1** *Along a line parallel to any of the two coordinate axis, i.e.  $\xi = \text{const.}$  or  $\eta = \text{const.}$ , we have a linear distribution of  $u$ . This allows us to prescribe at most two independent jumps in the solution across the interface, e.g.  $[u]_A$ ,  $[u]_B$  in Fig. 4 and 6. If the interface is not parallel to a coordinate axis we can and do prescribe one additional jump  $[u]_C$ , whereas otherwise we can and do prescribe two of these jumps.*

**Remark 3.2** *Along a line with  $n_\xi = \pm n_\eta$  (the interface cuts the cell in a  $\pm 45^\circ$ -angle) the normal gradient of  $u$ ,  $u_n = a_1 n_\xi + a_2 n_\eta + a_3 (\eta n_\xi + \xi n_\eta)$  for example, is constant! In that case we can prescribe only one independent jump in the normal derivative, e.g.  $[\beta u_n]_C$ , Fig. 4 and 6.*

A straightforward solution to determine the eight unknown coefficients would be to use the four corner values  $\underline{u} = [u_1, u_2, u_3, u_4]^t$  complemented with jump conditions  $[u]_A$ ,  $[u]_B$ ,  $[\beta u_n]_A$  and  $[\beta u_n]_B$ . However, it is obvious from Remark 3.2 that the resulting set of eight linear equations for  $\underline{x}$  has a singularity whenever  $a = b$ ,  $n_\xi = n_\eta = \frac{1}{\sqrt{2}}$  for cell type I as  $[\beta u_n]_A$  and  $[\beta u_n]_B$  are having the same set of coefficients in  $\underline{x}$ . The same singularity arises for cell type II if the interface crosses the cell diagonally.

Instead of using two jump conditions in  $[\beta u_n]$ , one could apply only one gradient jump condition with an additional jump in  $u$ , e.g.  $[\beta u_n]_C$  and  $[u]_C$ , in the midpoint  $C$  of the interface, see Fig. 4 and 6. However, due to Remark 3.1,  $[u]_C$  becomes a linear combination of  $[u]_A$  and  $[u]_B$  whenever  $a = b$  for type II and  $b = 1$ ,  $0 \leq a < 1$  or  $a = 1$ ,  $0 \leq b < 1$  for type I.

Another singularity arises for irregular cells of type I. For  $a = b = 1$  the interface touches the cell through the upper right point of the cell. In that case the interface points  $A$ ,  $B$ ,  $C$  merge into one single point leading to identical equations in  $[u]$  and  $[\beta u_n]$ .

The resulting set of linear equations for  $\underline{x}$  is not only unsolvable in any of the singular cases but the system becomes ill-conditioned in situations near the singularities. To remove all the discussed singularities, we propose a two-step asymptotic approach instead of trying to find the solution in a single step.

Instead of (10) we set

$$\begin{aligned} u^{(\mathfrak{A})}(\xi, \eta) &= u^{(\mathfrak{A},0)}(\xi, \eta) + \varepsilon u^{(\mathfrak{A},1)}(\xi, \eta) \\ u^{(\mathfrak{B})}(\tilde{\xi}, \tilde{\eta}) &= u^{(\mathfrak{B},0)}(\tilde{\xi}, \tilde{\eta}) + \varepsilon u^{(\mathfrak{B},1)}(\tilde{\xi}, \tilde{\eta}) \end{aligned} \quad (14)$$

with a properly defined small parameter  $\varepsilon$ . The functions  $u^{(\mathfrak{A},0)}$ ,  $u^{(\mathfrak{A},1)}$ ,  $u^{(\mathfrak{B},0)}$ , and  $u^{(\mathfrak{B},1)}$  will be constructed in such a way that the resulting solution is identical to the single step solution (10) in all non-singular situations. Our base solution will be a solution satisfying the interface conditions  $[u]_A$ ,  $[u]_B$ ,  $[u]_C$ , and  $[\beta u_n]_C$ .

### 3.4.1 A bilinear finite element for irregular cell type I

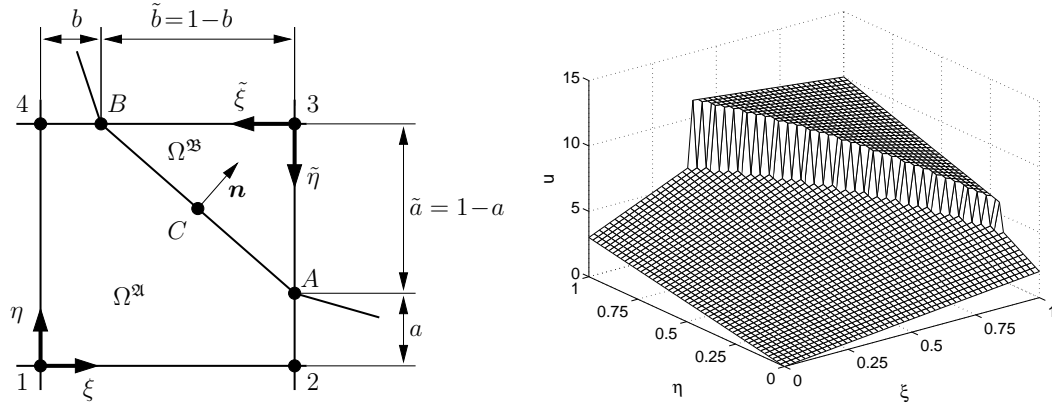


Figure 4. Irregular cell type I in the local  $\xi - \eta$  system with  $\xi, \eta \in [0, 1]$  (left). Typical solution for  $a = 0.2$ ,  $b = 0.4$ ,  $\beta^{\mathfrak{A}} = 1$ ,  $\beta^{\mathfrak{B}} = 1000$ ,  $u_1 = 0$ ,  $u_2 = 2$ ,  $u_3 = 10$ ,  $u_4 = 3$ ,  $[u]_A = -2$ ,  $[u]_B = -5$ ,  $[\beta u_n]_A = 10$ ,  $[\beta u_n]_B = 10$  (right).

In order to avoid the singularity discussed in remark 3.2 we introduce an additional point  $C$  in the middle of the interface, see Fig. 4. We prescribe jump conditions  $[u]_A$ ,  $[u]_B$ ,  $[u]_C = ([u]_A + [u]_B)/2$ , and  $[\beta u_n]_C = ([\beta u_n]_A + [\beta u_n]_B)/2$ . The small parameter  $\varepsilon$  in (14) is defined as

$$\varepsilon = \min(\tilde{a}, \tilde{b}).$$

To capture all singular cases  $\varepsilon = 0$  with the same leading order solution we need to define

$$\begin{aligned} [u]_A &= [u]_B, \text{ if } \varepsilon = 0 \text{ and } \tilde{b} = 0, \\ [u]_B &= [u]_A, \text{ if } \varepsilon = 0 \text{ and } \tilde{a} = 0. \end{aligned} \quad (15)$$

With this definition, we achieve that  $u^{(\mathfrak{A},0)}(1, 1) = u_3 - [u]_C$  for  $\varepsilon = 0$ . We

define the leading order solution to be constant in region  $\mathfrak{B}$  and bilinear in  $\mathfrak{A}$ :

$$\begin{aligned} u^{(\mathfrak{A},0)}(\xi, \eta) &= a_0^{(0)} + a_1^{(0)} \xi + a_2^{(0)} \eta + a_3^{(0)} \xi \eta, \\ u^{(\mathfrak{B},0)}(\tilde{\xi}, \tilde{\eta}) &= b_0^{(0)}. \end{aligned} \quad (16)$$

For the coefficients we get  $a_0^{(0)} = u_1$ ,  $a_1^{(0)} = u_2 - u_1$ ,  $a_2^{(0)} = u_4 - u_1$ ,  $a_3^{(0)} = u_1 - u_2 + u_3 - u_4 + [u]_C$ , and  $b_0^{(0)} = u_3$ . Including the zero valued coefficients on  $\mathfrak{B}$  we can write this as

$$\underline{x}^{(0)} = \left( \underline{\underline{A}}^{(0)} \right)^{-1} \underline{b} \quad (17)$$

with

$$\underline{x}^{(0)} = \begin{bmatrix} a_0^{(0)} \\ a_1^{(0)} \\ a_2^{(0)} \\ a_3^{(0)} \\ b_0^{(0)} \\ b_1^{(0)} \\ b_2^{(0)} \\ b_3^{(0)} \end{bmatrix}, \quad \left( \underline{\underline{A}}^{(0)} \right)^{-1} = \begin{bmatrix} 1 & 0 & 0 & 0 & 0 & 0 & 0 & 0 \\ -1 & 1 & 0 & 0 & 0 & 0 & 0 & 0 \\ -1 & 0 & 0 & 1 & 0 & 0 & 0 & 0 \\ 1 & -1 & 1 & -1 & \frac{1}{2} & \frac{1}{2} & 0 & 0 \\ 0 & 0 & 1 & 0 & 0 & 0 & 0 & 0 \\ 0 & \dots & & & \dots & 0 & & \\ \vdots & & & & & \vdots & & \\ 0 & \dots & & & \dots & 0 & & \end{bmatrix}, \quad \underline{b} = \begin{bmatrix} u_1 \\ u_2 \\ u_3 \\ u_4 \\ [u]_A \\ [u]_B \\ [\beta u_n]_A \\ [\beta u_n]_B \end{bmatrix} \quad (18)$$

**Remark 3.3** Using (15), the leading order solution is the correct solution  $u^{\mathfrak{A}} = u^{(\mathfrak{A},0)}$  in the limit  $\varepsilon = 0$ . We note that the constant solution  $u^{(\mathfrak{B},0)}$  does not cover any gradient  $u^{(\mathfrak{B},0)}$  for  $\varepsilon = 0$ ,  $\tilde{a} \neq 0$  or  $\varepsilon = 0$ ,  $\tilde{b} \neq 0$ . However, in those cases the interface is aligned with the boundary of the cell and the solution in region  $\mathfrak{B}$  does not have any influence on the evaluation of (6).

With the leading order solutions  $u^{(\mathfrak{A},0)}$  and  $u^{(\mathfrak{B},0)}$  we proceed to the first correction which is in our linear problem already the exact final solution. We make a full bilinear ansatz on both sides of the interface:

$$\begin{aligned} u^{(\mathfrak{A},1)}(\xi, \eta) &= a_0^{(1)} + a_1^{(1)} \xi + a_2^{(1)} \eta + a_3^{(1)} \xi \eta, \\ u^{(\mathfrak{B},1)}(\tilde{\xi}, \tilde{\eta}) &= b_0^{(1)} + b_1^{(1)} \hat{\tilde{\xi}} + b_2^{(1)} \hat{\tilde{\eta}} + b_3^{(1)} \hat{\tilde{\xi}} \hat{\tilde{\eta}}, \end{aligned} \quad (19)$$

where we have introduced a re-scaling

$$\hat{\tilde{\xi}} = \frac{\tilde{\xi}}{\tilde{b}}, \quad \hat{\tilde{\eta}} = \frac{\tilde{\eta}}{\tilde{b}}.$$

in region  $\mathfrak{B}$ . As the leading order solution covers already the four corner values of  $u$ , we get immediately  $a_0^{(1)} = a_1^{(1)} = a_2^{(1)} = b_0^{(1)} = 0$ . The missing four conditions for the remaining unknowns are the four jump conditions  $[u]_A^{(1)}$ ,  $[u]_B^{(1)}$ ,

$[u]_C^{(1)}$ , and  $[\beta u_n]^{(1)}$  at the interface, leading to the following set of equations:

$$\underline{x}^{(1)} = \left( \underline{\underline{A}}^{(1)} \right)^{-1} \underline{b}^{(1)}, \quad (20)$$

with

$$\begin{aligned} \underline{x}^{(1)} &= [a_0^{(1)}, a_1^{(1)}, a_2^{(1)}, a_3^{(1)}, b_0^{(1)}, b_1^{(1)}, b_2^{(1)}, b_3^{(1)}]^t \\ \underline{b}^{(1)} &= [0, 0, 0, 0, [u]_A^{(1)}, [u]_B^{(1)}, [u]_C^{(1)}, \varepsilon [\beta u_n]_C^{(1)}]^t \end{aligned}$$

and

$$\underline{\underline{A}}^{(1)} = \left[ \begin{array}{cccc|cccc} 1 & 0 & 0 & 0 & 0 & 0 & 0 & 0 \\ 0 & 1 & 0 & 0 & 0 & 0 & 0 & 0 \\ 0 & 0 & 1 & 0 & 0 & 0 & 0 & 0 \\ 0 & 0 & 0 & 0 & 1 & 0 & 0 & 0 \\ 0 & 0 & 0 & a & 0 & 0 & -1 & 0 \\ 0 & 0 & 0 & b & 0 & -1 & 0 & 0 \\ 0 & 0 & 0 & \frac{(1+a)(1+b)}{4} & 0 & -\frac{1}{2} & -\frac{1}{2} & -\frac{1}{4} \\ 0 & 0 & 0 & \frac{\varepsilon \beta^{2\mathfrak{A}} n_\xi (1+a)}{2\Delta x} + \frac{\varepsilon \beta^{2\mathfrak{A}} n_\eta (1+b)}{2\Delta y} & 0 & \frac{\varepsilon \beta^{2\mathfrak{B}} n_\xi}{\tilde{b}\Delta x} & \frac{\varepsilon \beta^{2\mathfrak{B}} n_\eta}{\tilde{a}\Delta y} & \frac{\varepsilon \beta^{2\mathfrak{B}} n_\xi}{\tilde{b}2\Delta x} + \frac{\varepsilon \beta^{2\mathfrak{B}} n_\eta}{\tilde{a}2\Delta y} \end{array} \right]$$

The last row of (20) – namely the jump condition  $[\beta u_n]^{(1)}$  – has been multiplied by  $\varepsilon$  to keep  $\underline{\underline{A}}^{(1)}$  non-singular in the limit  $\varepsilon \rightarrow 0$ . The non-zero elements of  $\underline{b}^{(1)}$  are given by

$$\begin{aligned} [u]_A^{(1)} &= \frac{[u]_A - [u]_A^{(0)}}{\varepsilon} \\ &= \frac{1}{\varepsilon} \left( [u]_A - (a_0^{(0)} + a_1^{(0)} + a_2^{(0)} a + a_3^{(0)} a - b_0^{(0)}) \right), \\ [u]_B^{(1)} &= \frac{[u]_B - [u]_B^{(0)}}{\varepsilon} \\ &= \frac{1}{\varepsilon} \left( [u]_B - (a_0^{(0)} + a_1^{(0)} b + a_2^{(0)} + a_3^{(0)} b - b_0^{(0)}) \right), \\ [u]_C^{(1)} &= \frac{[u]_C - [u]_C^{(0)}}{\varepsilon} \\ &= \frac{1}{\varepsilon} \left( [u]_C - (a_0^{(0)} + a_1^{(0)} \frac{1+b}{2} + a_2^{(0)} \frac{1+a}{2} + a_3^{(0)} \frac{(1+a)(1+b)}{4} - b_0^{(0)}) \right), \\ \varepsilon [\beta u_n]_C^{(1)} &= [\beta u_n]_C - [\beta u_n]_C^{(0)} \\ &= [\beta u_n]_C - \beta^{2\mathfrak{A}} \left( a_1^{(0)} \frac{n_\xi}{\Delta x} + a_2^{(0)} \frac{n_\eta}{\Delta y} + a_3^{(0)} \left( \frac{n_\xi(1+a)}{2\Delta x} + \frac{n_\eta(1+b)}{2\Delta y} \right) \right). \end{aligned} \quad (21)$$

Using the leading order solution (17) we can write  $\underline{b}^{(1)}$  with (21) as

$$\underline{b}^{(1)} = \underline{\underline{B}}_1 \underline{x}^{(0)} + \underline{\underline{B}}_2 \underline{b} = \left( \underline{\underline{B}}_1 \left( \underline{\underline{A}}^{(0)} \right)^{-1} + \underline{\underline{B}}_2 \right) \underline{b},$$

and further

$$\underline{x}^{(1)} = \left( \underline{\underline{A}}^{(1)} \right)^{-1} \underline{b}^{(1)} = \left( \underline{\underline{A}}^{(1)} \right)^{-1} \left( \underline{\underline{B}}_1 \left( \underline{\underline{A}}^{(0)} \right)^{-1} + \underline{\underline{B}}_2 \right) \underline{b}. \quad (22)$$

The matrices  $\underline{\underline{B}}_1$  and  $\underline{\underline{B}}_2$  are introduced to write  $\underline{b}^{(1)}$  in terms of  $\underline{x}^{(0)}$  and  $\underline{b}$ . They follow directly from (21) and are listed in the Appendix A.

The complete solution for an irregular cell type I can now be assembled using (14), (16), (17), (19) and (22):

$$\underline{x} = \underline{\underline{A}} \underline{b} = \left( (\underline{\underline{A}}^{(0)})^{-1} + \varepsilon (\underline{\underline{A}}^{(1)})^{-1} \left( \underline{\underline{B}}_1 (\underline{\underline{A}}^{(0)})^{-1} + \underline{\underline{B}}_2 \right) \right) \underline{b}, \quad (23)$$

Eq. (23) requires to invert  $\underline{\underline{A}}^{(1)}$ . Instead of using a two-step asymptotic approach one could calculate  $\underline{x}$  in a single step. However, the system becomes singular as  $\varepsilon \rightarrow 0$  due to the exposed reasons. Fig. 5 compares the condition number of matrix  $\underline{\underline{A}}^{(1)}$  from the asymptotic two-step scheme with the resulting matrix of a single step as a function of the small parameter  $\varepsilon$  and a ratio  $\beta^{21}/\beta^{23} = 1000$ . The condition number of the single-step solution quickly becomes extremely large. Our two-step asymptotic approach has an almost constant condition number for  $\varepsilon \rightarrow 0$  and has a well defined solution for  $\varepsilon = 0$ . The singularity is shifted from the set of linear equations to the small parameter  $\varepsilon$ . In the numerical implementation we need to evaluate the term  $1/\varepsilon$ , see (21). We get clean solutions for  $\varepsilon$  as small as  $r_{\min}$ , where  $r_{\min}$  is the smallest positive floating point number ( $r_{\min} = 2.2251 \times 10^{-308}$  for double precision floating point arithmetic on our machine). However, if  $\varepsilon < \text{eps}^2$ , where  $\text{eps}$  is the relative floating point accuracy, we set  $\underline{x} = \underline{x}^{(0)}$  and  $\underline{b} = \underline{b}^{(0)}$  and do not compute the next order solution. The asymptotic two-step solution is identical to the single-step solution with the exception that the asymptotic solution stays well behaved in the limit  $\varepsilon \rightarrow 0$ .

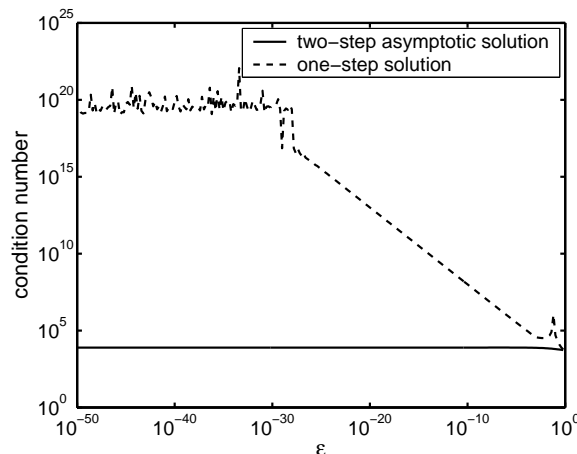


Figure 5. Condition number of matrix  $\underline{\underline{A}}^{(1)}$  in comparison with the resulting matrix from a one-step solution and a ratio  $\beta^{21}/\beta^{23} = 1000$ .

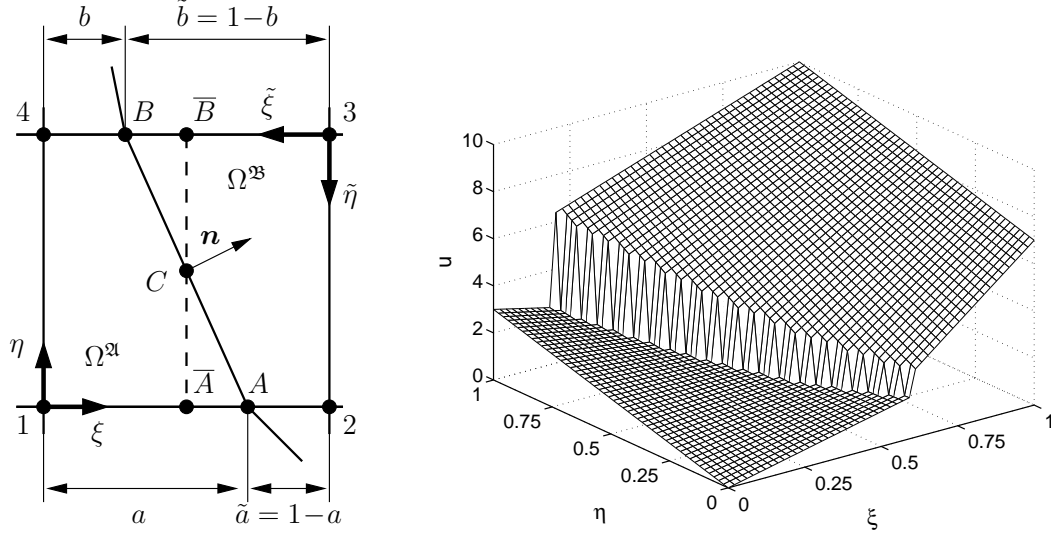


Figure 6. Irregular cell type II in the local  $\xi - \eta$  system with  $\xi, \eta \in [0, 1]$  (left). Solution for  $a = 0.6$ ,  $b = 0.2$ ,  $\beta^{\mathfrak{A}} = 100$ ,  $\beta^{\mathfrak{B}} = 1$ ,  $u_1 = 0$ ,  $u_2 = 7$ ,  $u_3 = 10$ ,  $u_4 = 3$ ,  $[u]_A = -1, [u]_B = -4$ ,  $[\beta u_n]_A = 1$ ,  $[\beta u_n]_B = 10$  (right)

### 3.4.2 A bilinear finite element for irregular cell type II

The construction of a non-singular bilinear finite element for an irregular cell of type II, Fig. 6, follows the lines presented in the preceding section for type I. Again, our base solution will be constructed with three prescribed solution jumps  $[u]$  and one gradient jump  $[\beta u_n]$  across the interface. This ensures identical solutions for type I and type II cells under conditions  $a = 0$ ,  $b \in [0, 1]$  for type I and  $a = 1$ ,  $b \in [0, 1]$  for type II, respectively. However, as pointed out in Remark 3.1, we cannot prescribe three independent jump conditions  $[u]$  if  $a = b$ , i.e. the interface cuts the cell perpendicular to the  $\xi$ -axis. To resolve this singularity we apply the two-step asymptotic approach (14) with the small parameter now defined as

$$\varepsilon = (a - b).$$

We use a bilinear ansatz function for the leading order solution on both sides of the interface

$$\begin{aligned} u^{(\mathfrak{A},0)}(\xi, \eta) &= a_0^{(0)} + a_1^{(0)} \xi + a_2^{(0)} \eta + a_3^{(0)} \xi \eta, \\ u^{(\mathfrak{B},0)}(\tilde{\xi}, \tilde{\eta}) &= b_0^{(0)} + b_1^{(0)} \tilde{\xi} + b_2^{(0)} \tilde{\eta} + b_3^{(0)} \tilde{\xi} \tilde{\eta}. \end{aligned} \quad (24)$$

The leading order solution is determined by the four corner values of  $u$  and the jump conditions  $[u]_{\bar{A}}$ ,  $[u]_{\bar{B}}$ ,  $[\beta u_n]_{\bar{A}}$ , and  $[\beta u_n]_{\bar{B}}$ . Points  $\bar{A}$  and  $\bar{B}$  are defined to have the same  $\xi$ -coordinate as point  $C$ , i.e.  $\xi_{\bar{A}} = \xi_{\bar{B}} = \xi_C = (a + b)/2$ , so that  $\bar{A} = A$  and  $\bar{B} = B$  in the limit  $\varepsilon = 0$ , see Fig. 6. Therefore, the imaginary leading order interface has a unit normal vector  $\mathbf{n}^{(0)} = [1, 0]^t$ . The coefficients  $a_0^{(0)} = u_1$ ,  $a_2^{(0)} = u_4 - u_1$ ,  $b_0^{(0)} = u_3$ , and  $b_2^{(0)} = u_2 - u_3$  are defined by the corner

values. With a unit normal vector  $\mathbf{n}^{(0)} = [1, 0]^t$  for the leading order solution we have quasi one-dimensional distributions of  $u$  along  $\eta = \text{const}$  lines. The solution for the remaining coefficients is (see also [10,14])

$$\begin{aligned} a_1^{(0)} &= \frac{\beta^{\mathfrak{B}}}{\delta} \left( -u_1 + u_2 \quad + [u]_A \quad - \frac{(1-c)\Delta x}{\beta^{\mathfrak{B}}} \quad [\beta u_n]_A \right), \\ b_1^{(0)} &= \frac{-\beta^{\mathfrak{A}}}{\delta} \left( -u_1 + u_2 \quad + [u]_A \quad + \frac{c\Delta x}{\beta^{\mathfrak{A}}} \quad [\beta u_n]_B \right), \\ a_3^{(0)} &= \frac{\beta^{\mathfrak{B}}}{\delta} \left( u_1 - u_2 + u_3 - u_4 - [u]_A + [u]_B - \frac{(1-c)\Delta x}{\beta^{\mathfrak{B}}} \left( [\beta u_n]_A - [\beta u_n]_B \right) \right), \\ b_3^{(0)} &= \frac{-\beta^{\mathfrak{A}}}{\delta} \left( -u_1 + u_2 - u_3 + u_4 + [u]_A - [u]_B + \frac{(1-c)\Delta x}{\beta^{\mathfrak{A}}} \left( [\beta u_n]_A - [\beta u_n]_B \right) \right), \end{aligned}$$

with  $\delta = \beta^{\mathfrak{B}}(a+b)/2 + \beta^{\mathfrak{A}}((1-a) + (1-b))/2$ . For later purposes, we write the leading order solution in matrix form

$$\underline{x}^{(0)} = \left( \underline{\underline{A}}^{(0)} \right)^{-1} \underline{b} \quad (25)$$

with

$$\underline{x}^{(0)} = \begin{bmatrix} a_0^{(0)} \\ a_1^{(0)} \\ a_2^{(0)} \\ a_3^{(0)} \\ b_0^{(0)} \\ b_1^{(0)} \\ b_2^{(0)} \\ b_3^{(0)} \end{bmatrix}, \quad \left( \underline{\underline{A}}^{(0)} \right)^{-1} = \begin{bmatrix} 1 & 0 & 0 & 0 & 0 & 0 & 0 & 0 \\ -\delta^{\mathfrak{A}} & \delta^{\mathfrak{A}} & 0 & 0 & \delta^{\mathfrak{A}} & 0 & \delta^{\mathfrak{A}}\gamma^{\mathfrak{A}} & 0 \\ -1 & 0 & 0 & 1 & 0 & 0 & 0 & 0 \\ \delta^{\mathfrak{A}} & -\delta^{\mathfrak{A}} & \delta^{\mathfrak{A}} & -\delta^{\mathfrak{A}} & -\delta^{\mathfrak{A}} & \delta^{\mathfrak{A}} & -\delta^{\mathfrak{A}}\gamma^{\mathfrak{A}} & \delta^{\mathfrak{A}}\gamma^{\mathfrak{A}} \\ 0 & 0 & 1 & 0 & 0 & 0 & 0 & 0 \\ 0 & 0 & \delta^{\mathfrak{B}} & -\delta^{\mathfrak{B}} & 0 & \delta^{\mathfrak{B}} & 0 & -\delta^{\mathfrak{B}}\gamma^{\mathfrak{B}} \\ 0 & 1 & -1 & 0 & 0 & 0 & 0 & 0 \\ -\delta^{\mathfrak{B}} & \delta^{\mathfrak{B}} & -\delta^{\mathfrak{B}} & \delta^{\mathfrak{B}} & \delta^{\mathfrak{B}} & -\delta^{\mathfrak{B}} & -\delta^{\mathfrak{B}}\gamma^{\mathfrak{B}} & \delta^{\mathfrak{B}}\gamma^{\mathfrak{B}} \end{bmatrix},$$

$$\underline{b} = [u_1, u_2, u_3, u_4, [u]_A, [u]_B, [\beta u_n]_A, [\beta u_n]_B]^t, \quad (26)$$

and  $\delta^{\mathfrak{A}} = \beta^{\mathfrak{B}}/\delta$ ,  $\delta^{\mathfrak{B}} = -\beta^{\mathfrak{A}}/\delta$ ,  $\delta = (\xi_C \beta^{\mathfrak{B}} + \tilde{\xi}_C \beta^{\mathfrak{A}})$ ,  $\gamma^{\mathfrak{A}} = \frac{\tilde{\xi}_C \Delta x}{\beta^{\mathfrak{B}}}$ ,  $\gamma^{\mathfrak{B}} = \frac{\xi_C \Delta x}{\beta^{\mathfrak{A}}}$ . Furthermore, we define  $[u]_C = ([u]_A + [u]_B)/2$ .

We use a similar bilinear ansatz for the correction as in (19):

$$\begin{aligned} u^{(\mathfrak{A},1)}(\xi, \eta) &= a_0^{(1)} + a_1^{(1)} \xi + a_2^{(1)} \eta + a_3^{(1)} \xi \eta, \\ u^{(\mathfrak{B},1)}(\tilde{\xi}, \tilde{\eta}) &= b_0^{(1)} + b_1^{(1)} \tilde{\xi} + b_2^{(1)} \tilde{\eta} + b_3^{(1)} \tilde{\xi} \tilde{\eta}, \end{aligned} \quad (27)$$

where the leading order solution with (14) immediately yields  $a_0^{(1)} = a_2^{(1)} = b_0^{(1)} = b_2^{(1)} = 0$ . The remaining coefficients are calculated using the four jump

conditions at the interface, with the first three of them

$$\begin{aligned}
[u]_A^{(1)} &= \frac{[u]_A - [u]_A^{(0)}}{\varepsilon} \\
&= \frac{1}{\varepsilon} \left( [u]_A - (a_0^{(0)} + a_1^{(0)} a - b_0^{(0)} - b_1^{(0)} \tilde{a} - b_2^{(0)} - b_3^{(0)} \tilde{a}) \right), \\
[u]_B^{(1)} &= \frac{[u]_B - [u]_B^{(0)}}{\varepsilon} \\
&= \frac{1}{\varepsilon} \left( [u]_B - (a_0^{(0)} + a_1^{(0)} b + a_2^{(0)} + a_3^{(0)} b - b_0^{(0)} - b_1^{(0)} \tilde{b}) \right), \\
[\beta u_n]_C^{(1)} &= \frac{[\beta u_n]_C - [\beta u_n]_C^{(0)}}{\varepsilon} \\
&= \frac{1}{\varepsilon} \left( [\beta u_n]_C - \beta^{\mathfrak{A}} \left( a_1^{(0)} \frac{n_\xi}{\Delta x} + a_2^{(0)} \frac{n_\eta}{\Delta y} + a_3^{(0)} \left( \frac{n_\xi}{2\Delta x} + \frac{n_\eta(a+b)}{2\Delta y} \right) \right) \right. \\
&\quad \left. - \beta^{\mathfrak{B}} \left( b_1^{(0)} \frac{n_\xi}{\Delta x} + b_2^{(0)} \frac{n_\eta}{\Delta y} + b_3^{(0)} \left( \frac{n_\xi}{2\Delta x} + \frac{n_\eta(\tilde{a}+\tilde{b})}{2\Delta y} \right) \right) \right).
\end{aligned} \tag{28}$$

We do not want to use jump condition  $[u]_C$  directly as we have  $[u]_C^{(1)} \rightarrow ([u]_A^{(1)} + [u]_B^{(1)})/2$  in the limit  $\varepsilon \rightarrow 0$  making the resulting equation a linear combination of the two other jump conditions. Instead, we use  $[u]_C$  in the following form

$$\Delta[u] = [u]_C - \frac{1}{2}([u]_A + [u]_B) = -\varepsilon \left( \frac{a_3 - b_3}{4} \right).$$

This leads us to the fourth condition for the unknown coefficients:

$$\Delta[u]^{(1)} = [u]_C^{(1)} - \frac{1}{2}([u]_A^{(1)} + [u]_B^{(1)}) = \frac{\Delta[u] - \Delta[u]^{(0)}}{\varepsilon} = -\frac{a_3^{(0)} - b_3^{(0)}}{\varepsilon}. \tag{29}$$

Taking into account the known zero values of some of the coefficients, the complete set of linear equations can now be written as

$$\underline{x}^{(1)} = (\underline{A}^{(1)})^{-1} \underline{b}^{(1)}$$

with

$$\underline{A}^{(1)} = \left[ \begin{array}{cccc|cccc}
1 & 0 & 0 & 0 & 0 & 0 & 0 & 0 \\
0 & 0 & 1 & 0 & 0 & 0 & 0 & 0 \\
0 & 0 & 0 & 0 & 1 & 0 & 0 & 0 \\
0 & 0 & 0 & 0 & 0 & 0 & 1 & 0 \\
0 & a & 0 & 0 & 0 & -\tilde{a} & 0 & -\tilde{a} \\
0 & b & 0 & b & 0 & -\tilde{b} & 0 & 0 \\
0 & 0 & 0 & 1/4 & 0 & 0 & 0 & -1/4 \\
0 & \frac{\beta^{\mathfrak{A}} n_\xi}{\Delta x} & 0 & \frac{\beta^{\mathfrak{A}} n_\xi}{2\Delta x} + \frac{\beta^{\mathfrak{A}} n_\eta(a+b)}{2\Delta y} & 0 & \frac{\beta^{\mathfrak{B}} n_\xi}{\Delta x} & \frac{\beta^{\mathfrak{B}} n_\xi}{2\Delta x} + \frac{\beta^{\mathfrak{B}} n_\eta(\tilde{a}+\tilde{b})}{2\Delta y} & 0
\end{array} \right],$$

$$\underline{x}^{(1)} = [a_0^{(1)}, a_1^{(1)}, a_2^{(1)}, b_3^{(1)}, b_0^{(1)}, b_1^{(1)}, b_2^{(1)}, b_3^{(1)}]^t,$$

and

$$\underline{b}^{(1)} = [0, 0, 0, 0, [u]_A^{(1)}, [u]_B^{(1)}, \Delta[u]^{(1)}, [\beta u_n]_C^{(1)}]^t.$$

The non-zero elements of  $\underline{b}^{(1)}$  are given by the right hand sides of (28) and (29). Instead of solving for  $\underline{x}^{(1)}$  we solve directly for  $\varepsilon \underline{x}^{(1)}$ . Doing so, factors of  $1/\varepsilon$  in (28) and (29) cancel and we do not need to divide by  $\varepsilon$  at any point for this type of element. With the leading order solution  $\underline{x}^{(0)}$  and the correction  $\varepsilon \underline{x}^{(1)}$  we assemble the complete solution following the lines presented in Section 3.4.1 and end with

$$\underline{x} = \underline{A} \underline{b} = \left( (\underline{A}^{(0)})^{-1} + (\underline{A}^{(1)})^{-1} \left( \underline{B}_1 (\underline{A}^{(0)})^{-1} + \underline{B}_2 \right) \right) \underline{b}. \quad (30)$$

The matrices  $\underline{B}_1$  and  $\underline{B}_2$  are again introduced to write the correction solution  $\underline{b}^{(1)}$  in terms of  $\underline{x}^{(0)}$  and  $\underline{b}$  and are provided in the Appendix B.

Fig. 7 shows the condition number for matrix  $\underline{A}^{(1)}$  as a function of the parameter  $\varepsilon$  and compares it with the condition number of the matrix resulting from a one-step solution. The condition number in the two-step asymptotic scheme is almost independent of  $\varepsilon$ , whereas the condition number for the one-step solution scales inverse proportional to  $\varepsilon$ . We note that with increasing condition number the difference between the two-step asymptotic solution and the single-step increases making the one-step solution useless in the limit  $\varepsilon \rightarrow 0$ .

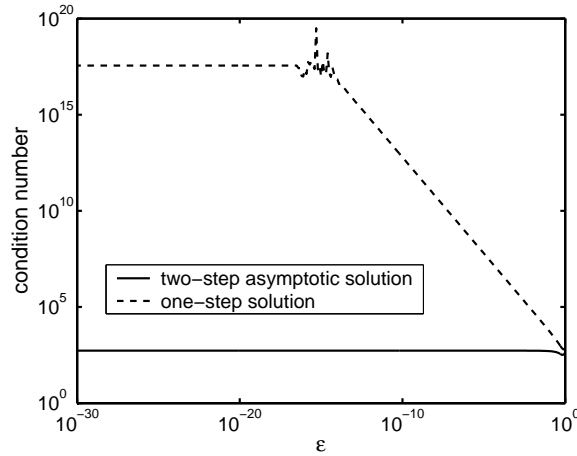


Figure 7. Condition number of matrix  $\underline{A}^{(1)}$  in comparison with the resulting matrix from a one-step solution and a ratio  $\beta^{21}/\beta^{23} = 1000$ .

## 4 Numerical results

In following examples we compare numerical results with given analytic solutions  $u^+(\mathbf{x})$  and  $u^-(\mathbf{x})$  and corresponding coefficients  $\beta^+(\mathbf{x})$  and  $\beta^-(\mathbf{x})$ .

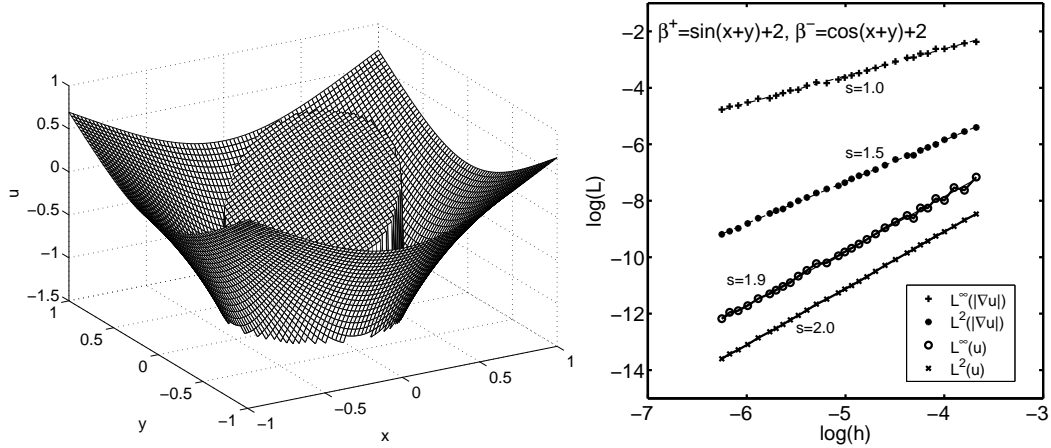


Figure 8. Solution for example 1 with  $80 \times 80$  grid-points (left). Convergence results for the solution  $u$  and the gradient  $|\nabla u|$  in the  $L^\infty$  and  $L^2$ -norm (right).

We use the analytic solution to provide the right hand side  $f(\mathbf{x})$  in (1) and to prescribe jump conditions  $[u]$  and  $[\beta u_n]$  at positions where the interface  $\Gamma$  crosses grid lines. Furthermore, the analytic solution provides us with the proper Dirichlet boundary conditions. The interface is defined by the zero level of the signed normal distance function  $\phi(\mathbf{x})$ . We set  $\Omega^+$  and  $\Omega^-$  to be the region with  $\phi(\mathbf{x}) > 0$  and  $\phi(\mathbf{x}) < 0$ , respectively. The position of the interface has been evaluated assuming linear distributions of  $\phi$  between grid points. The unit normal vector pointing from  $\Omega^+$  to  $\Omega^-$  is given by  $\mathbf{n} = -\frac{\nabla \phi}{|\nabla \phi|}$ . The arising linear system of equations have all been solved with the `hypre` library [2] using a BICGSTAB solver with an algebraic multigrid preconditioner.

#### 4.1 Example 1

This example is taken from [3]. We solve (1) in the domain  $-1 \leq x, y \leq 1$ . The interface is a simple circle with radius 0.5 and midpoint at  $(0, 0)$ . The analytic solutions  $u^\pm$ , the coefficients  $\beta^\pm$ , and the level set function are given as follows:

$$\begin{aligned} u^+ &= \ln(x^2 + y^2), & u^- &= \sin(x + y), \\ \beta^+ &= \sin(x + y) + 2, & \beta^- &= \cos(x + y) + 2, \\ \phi &= \sqrt{(x^2 + y^2)} - 0.5. \end{aligned}$$

The solution as well as the the normal derivative are discontinuous across the interface. This example is characterized by a simple geometry of the interface and a small difference between the coefficients  $\beta^+$  and  $\beta^-$ . Fig. 8 shows the numerical solution of the method using  $80 \times 80$  grid-points. A convergence study with two different sets of grids – one with  $\Delta x/\Delta y = 1$  and the other with  $\Delta x/\Delta y = 3$  – is summarized in Table 4.1. The method achieves 2nd

Grid	$L^2$	Order	$L^\infty$	Order
$64 \times 64$	2.9251e-04		1.8234e-03	
$128 \times 128$	6.9066e-05	2.08	4.3578e-04	2.06
$256 \times 256$	1.7387e-05	1.99	1.2602e-04	1.79
$512 \times 512$	4.3486e-06	2.00	3.1314e-05	2.01
$1024 \times 1024$	1.0923e-06	1.99	8.4610e-06	1.89
$40 \times 120$	3.8655e-04		1.41177e-03	
$80 \times 240$	9.5271e-05	2.02	3.52939e-04	2.00
$160 \times 480$	2.3659e-05	2.01	9.24177e-05	1.93
$320 \times 960$	5.9741e-06	1.99	2.47270e-05	1.90
$640 \times 1920$	1.5876e-06	1.91	6.81066e-06	1.86

Table 1

Convergence results for the solution  $u$  in the  $L^2$  and  $L^\infty$ -norm for example 1 on two different sets of grids;  $\Delta x = \Delta y$  first set,  $\Delta x/\Delta y = 3$  second set.

order of accuracy in the  $L^2$ , and  $L^\infty$  norm on both sets of grids. Our results are comparable to the ones presented in [3] with a smaller error constant reported in [3]. However, using triangulated Cartesian grids in [3], the interface is resolved with almost twice as many points as in our method on an identical underlying Cartesian grid. This example shows a smooth second order behavior for the error with decreasing grid spacing. However, it is known for interface problems that the error does not necessarily behave monotonically under grid refinement. Therefore, the asymptotic convergence rate is usually defined as the slope of the linear least square fit of the error over mesh size in a log-log diagram. Fig. 8 plots the maximum error  $L^\infty$  as well as the error in the  $L^2$  norm over mesh size  $h = \Delta x = \Delta y$  for the solution  $u$  and the norm of the gradient  $|\nabla u|$ . The results have been obtained on 30 different grids ranging from  $80 \times 80$  to  $1040 \times 1040$  grid points. The slopes of the least square fit are  $s = 2.0$  and  $s = 1.9$  in the  $L^2$  and  $L^\infty$  norm for the solution values  $u$ , respectively. As expected, with a value of 1.0 we lose one order of accuracy for the gradient in the  $L^\infty$  norm whereas we see an order of accuracy of 1.5 in the  $L^2$  norm. The gradients have been evaluated in the midpoints of our bilinear cells, i. e.  $\xi = \eta = \tilde{\xi} = \tilde{\eta} = 0.5$ .

## 4.2 Example 2

This case follows an example investigated by Li in [7]. The position of the interface is given in parametric form

$$\begin{aligned} X(\theta) &= r(\theta) \cos(\theta) + x_0, \\ Y(\theta) &= r(\theta) \sin(\theta) + y_0, \end{aligned} \quad 0 \leq \theta \leq 2\pi, \quad (31)$$

with

$$r(\theta) = r_0 + r_1 \sin(\omega\theta), \quad 0 \leq \theta \leq 2\pi.$$

The parameters are set to  $r_0 = 0.5$ ,  $r_1 = 0.2$ ,  $\omega = 5$ , and  $x_0 = y_0 = 0.2/\sqrt{20}$ . The analytic solution on the computational domain  $-1 \leq x, y \leq 1$  is given as

$$\begin{aligned} u^+ &= \frac{r^4 + C_0 \log(2r)}{\beta^+}, \quad u^- = \frac{r^2}{\beta^-}, \\ \beta^+ &= \text{const.}, \quad \beta^- = \text{const.}, \end{aligned}$$

where  $r = \sqrt{(x - x_0)^2 + (y - y_0)^2}$  and  $C_0 = -0.1$ . Fig. 9 shows solutions on grids with  $100 \times 100$  points and convergence results for three different sets of coefficients  $\beta^+$ ,  $\beta^-$ . A characteristic feature of this example is that the solution becomes constants in regions with large  $\beta$  values, which is clearly seen for the second and third case in Fig. 9 with  $\beta^+ = 1000$ ,  $\beta^- = 1$  and  $\beta^+ = 1$ ,  $\beta^- = 1000$ , respectively.

The convergence results in Fig. 9 have been obtained on 30 different meshes having  $80 \times 80$  up to  $1040 \times 1040$  grid points. In all three cases we see a sharp drop of the error on the coarsest grids indicating a poorly resolved interface. We left those results out in the evaluation of the convergence rates. The observed convergence rates – or rather the slopes  $s$  of the linear least square fit – vary between 2.0 – 2.2 in the  $L^2$  norm and 1.8 – 1.9 in the  $L^\infty$  norm for the solution values  $u$  indicating locally second order of accuracy even for large ratios of the coefficients  $\beta^+$  and  $\beta^-$ . Furthermore, we observe a strongly non-monotonic behavior of the maximum error  $l^\infty$  under grid refinement. This can be explained by the fact that the control points of the interface on a Cartesian grid using a level set approach – namely the points where the interface cuts grid lines – are non-uniformly spaced and that the distribution of those control points might get locally more unequal under grid refinement. Similar behavior has been observed in [7]. As in example 1 we have for the gradient of  $u$  an order of accuracy of 1 in the  $L^\infty$  norm. In this example we see with values between 1.6 and 1.8 almost second order convergence of the gradient in the  $L^2$  norm. The qualitative similarity between the curves for  $u$  and  $|\nabla u|$  is apparent.

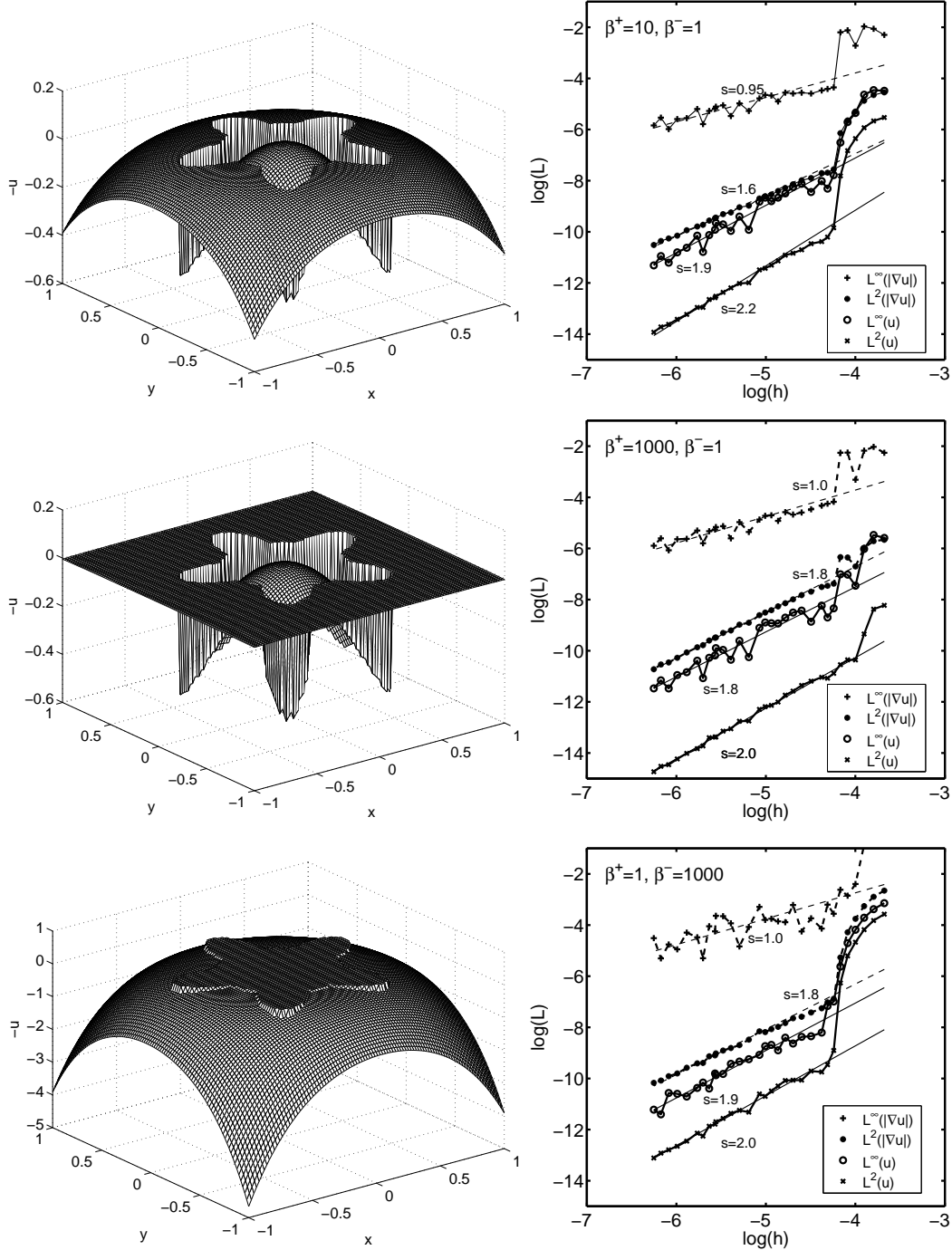


Figure 9. Solutions for example 2 on  $100 \times 100$  grids for different values of  $\beta^+$ ,  $\beta^-$  (left) and corresponding convergence results in the  $L^\infty$  and  $L^2$  norm for the solution  $u$  and its gradient  $|\nabla u|$  (right).

#### 4.2.1 A note on CPU times

All of the linear system of equations in this study have been solved with the freely available hypre package [2]. We have used both the algebraic multi-

grid solver BoomerAMG as a direct solver and in as a preconditioner for the BICGSTAB algorithm. Table 2 shows some CPU times for Example 2 on different grids and different ratios of the coefficients  $\beta$ . We have used the standard parameters of the hypr package with the exception of the strong threshold value, which we have changed from its default value 0.25 to 0.9, and the number of multigrid cycles which has been set to 15 when we using the AMG as a preconditioner. From Table 2 it is apparent that the AMG as a direct solver is much faster than the combined BICGSTAB and AMG, but we where not able to get solutions with the AMG alone in cases of high ratios of the coefficients of 1000 and above. One can also observe that in many cases the CPU time scales almost linearly with the problem size which is a feature of fast solvers. Furthermore, from the results in Table 2 we see that the CPU time increases with increasing ratio of the coefficients  $\beta$ . Although all the results in Table 2 have been calculated with the same set of parameters, we remark that occasionally in cases of very high ratios of the coefficients the AMG preconditioned BICGSTAB does not converge. In those cases it is necessary to modify some of the build-parameters of the solver. The same experience has been reported in [8]. However, the numbers in Table 2 might change dramatically as we did not try to find the fastest combination of parameters. The construction of efficient solvers for elliptic problems with discontinuities and high ratios of the coefficients is still an open research area.

### 4.3 Example 3

In the third example, the interface is again given by equation (31) with the following set of parameters:  $x_0 = 0.1$ ,  $y_0 = 1.2$ ,  $r_0 = 0.5$ ,  $r_1 = 0.15$ , and  $\omega = 4$ . The solution domain is a square defined by  $-1 \leq x \leq 1$  and  $0 \leq y \leq 2$ . The exact solution is adapted from [7]:

$$\begin{aligned} u^+ &= e^x (x^2 \sin(y) + y^2), \\ u^- &= -(x^2 + y^2). \end{aligned}$$

In contrast to [7] we have varying coefficients

$$\begin{aligned} \beta^+ &= 1000 (x y + 5), \\ \beta^- &= 1 + x^2 + y^2. \end{aligned}$$

The maximum ratio  $\beta^+/\beta^-$  at the interface is about 3600 and the smallest about 1100. Compared to example 2 the solution is independent of the coefficient  $\beta$ . However, the magnitude of the jump  $[\beta u_n]$  increases with the jump  $[\beta]$ .

grid	$\beta^+$	$\beta^-$	CPU time [s]	
			BICGSTAB + AMG	AMG
128 × 128	1	1	0.4	0.03
256 × 256	1	1	1.7	0.15
512 × 512	1	1	6.9	0.64
1024 × 1024	1	1	27.8	2.62
128 × 128	1	10	0.5	0.05
256 × 256	1	10	2.5	0.18
512 × 512	1	10	10.2	1.01
1024 × 1024	1	10	41.4	2.97
128 × 128	10	1	0.6	0.05
256 × 256	10	1	2.6	0.19
512 × 512	10	1	10.3	0.79
1024 × 1024	10	1	41.4	4.04
128 × 128	1	100	0.6	0.07
256 × 256	1	100	2.6	0.38
512 × 512	1	100	20.7	1.47
1024 × 1024	1	100	82.4	5.06
128 × 128	100	1	0.6	0.12
256 × 256	100	1	2.6	0.31
512 × 512	100	1	10.3	2.04
1024 × 1024	100	1	41.3	8.10
128 × 128	1	1000	1.7	–
256 × 256	1	1000	13.6	–
512 × 512	1	1000	61.0	–
1024 × 1024	1	1000	123.2	–
128 × 128	1000	1	3.7	–
256 × 256	1000	1	12.7	–
512 × 512	1000	1	41.0	–
1024 × 1024	1000	1	343.2	–

Table 2

CPU times for Example 2 on different grids and different ratios of the coefficients for example 2.

Fig. 10 shows the numerical solution on a  $100 \times 100$  grid and convergence results in the  $L^\infty$  and  $L^2$  norm. The asymptotic convergence rates for the solution values are 2.1 in the  $L^2$  norm and 1.8 in the  $L^\infty$  norm showing again locally second order of accuracy of the method. As in the examples before, we see again an order of accuracy of 1 for the gradient in the  $L^\infty$  norm and a slightly better value of 1.5 in the  $L^2$  norm.

#### 4.4 Example 4

This example is taken from Hou and Liu [3]. The interface is a cardioid with a level set function given by

$$\phi(x, y) = \left(3(x^2 + y^2) - x\right)^2 - x^2 - y^2.$$

The specific feature of this example is the singular point of the interface with a cusp point at  $x = y = 0$ , Fig. 11. The analytic solutions  $u^\pm$ , the coefficients

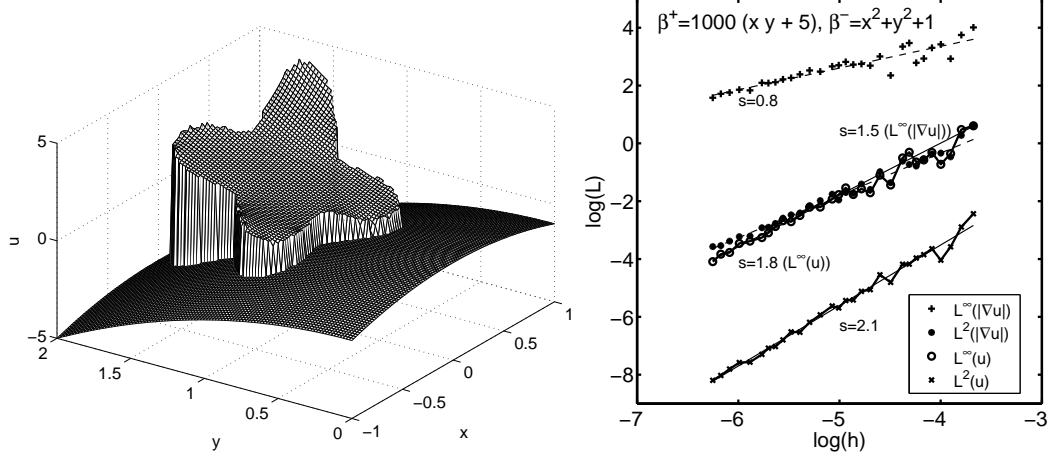


Figure 10. Solution for example 3 on a 100 grid (left) and convergence results for the solution  $u$  and its gradient  $|\nabla u|$  in the  $L^\infty$  and  $L^2$  norm (right).

$\beta^\pm$ , and the level set function are given as follows:

$$\begin{aligned} u^+ &= 1 - x^2 - y^2, & u^- &= x^2 + y^2 + 2, \\ \beta^+ &= x^2 - y^2 + 3, & \beta^- &= xy + 3. \end{aligned}$$

Fig. 11 shows the numerical solution on a grid with  $100 \times 100$  grid points and

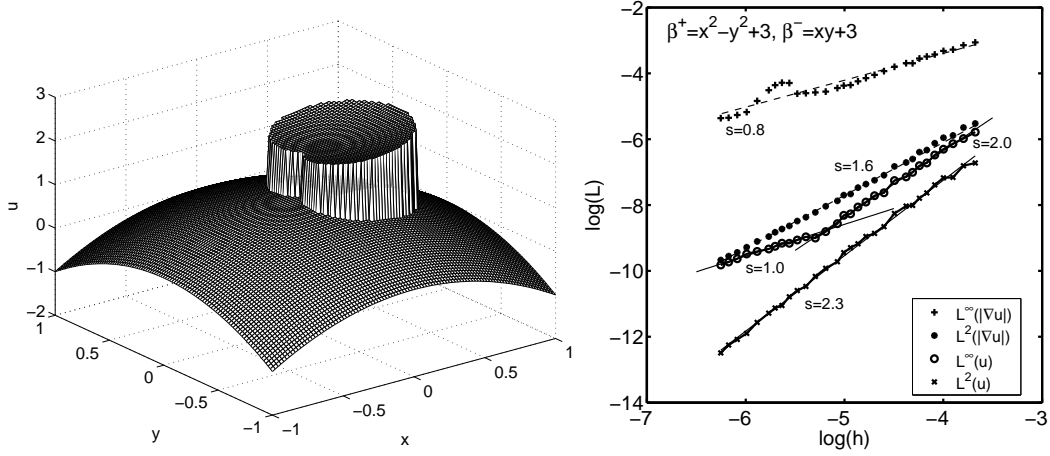


Figure 11. Solution for example 4 on a  $100 \times 100$  grid (left) and convergence study for the error in the  $L^\infty$  and  $L^2$  norm (right).

results of a convergence study on 35 grids ranging from  $80 \times 80$  to  $1040 \times 1040$  grid points. Since this is a non-smooth interface at the cusp point, we cannot expect second order convergence in the  $L^\infty$  norm for the solution values of  $u$ . The convergence results in Fig. 11 demonstrate second order convergence in the  $L^\infty$  norm on the coarser grids comparable to those used by Hou and Liu [3], and first order on finer grids which resolve the cusp. We find second order convergence on all grids in the  $L^\infty$  norm if we exclude the area around the cusp

point. Corresponding to the abrupt change in the convergence order for the solution  $u$  we see an interim increase of the error in the gradient. The overall order of convergence for the gradient in the  $L^\infty$  has been evaluated to a value of 0.8 for this problem. The  $L^2$  norm indicates second order convergence on all grids for the solution  $u$  and a convergence order of 1.6 for the gradient  $|\nabla u|$ .

## 5 Conclusion

We have developed a second-order accurate method for the solution of the Poisson equation with variable coefficients and discontinuities across embedded interface. The interface is represented by a level set approach. In contrast to existing methods in the literature we use a finite volume approach on Cartesian grids using ideas from finite element methods in reconstructing the solution within grid cells. We have presented a bilinear finite element for irregular cut cells taking into account known jump conditions of the solution and the normal gradient across the interface. We resolve singularities arising from the bilinear ansatz itself and the position of the interface relative to the grid by a two-step asymptotic approach. Although the subject of this work is the numerical solution of a Poisson equation type of problem we note that our bilinear finite element might be equally useful for the reconstruction of any other discontinuous function on Cartesian grids (e. g.: the velocity field in premixed combustion). Our discretisation leads to a compact nine-point stencil for the discrete Laplacian, with appropriately adjusted weights near the interface. The resulting set of linear equations is symmetric and positive definite in case of constant and equal coefficients. Detailed numerical investigations have revealed the matrix in the general case of variable coefficients to be slightly non-symmetric. As a solver for the resulting set of linear equations we have used a black box algebraic multigrid solver. The method in principle can be extended to three spatial dimensions where we have four different types of irregular cells.

## References

- [1] Z. Chen and J. Zou. Finite element methods and their convergence for elliptic and parabolic interface problems. *Numerische Mathematik*, 79:175–202, 1998.
- [2] R.D. Falgout and U.M. Yang. hypre: a library of high performance preconditioners. In P.M.A. Sloot, C.J.K. Tan, J.J. Dongarra, and A.G. Hoekstra, editors, *Computational Science - ICCS 2002 Part III*, volume 2331 of *Lecture Notes in Computer Science*, pages 632–641. Springer-Verlag, 2002.

- [3] S. Hou and X. Liu. A numerical method for solving variable coefficient elliptic equation with interfaces. *Journal of Computational Physics*, 202:411–445, 2005.
- [4] H. Johansen and P. Colella. A cartesian grid embedded boundary method for poisson’s equation on irregular domains. *Journal of Computational Physice*, 147:60–85, 1998.
- [5] R. J. LeVeque and Z. Li. The Immersed Interface Method for Elliptic Equations with Discontinuous Coefficients and Singular Sources. *SIAM Journal on Numerical Analysis*, 31(4):1019–1044, 1994.
- [6] R. J. LeVeque and Z. Li. Immersed Interface Methods for Stokes Flow with Elastic Boundaries or Surface Tension. *SIAM Journal on Scientific Computing*, 18:709–735, 1997.
- [7] Z. Li. A fast iterative algorithm for elliptic interface problems. *SIAM Journal of Numerical Analysis*, 35(1):230–254, 1998.
- [8] Z. Li and K. Ito. Maximum principle preserving schemes for interface problems with discontinuous coefficients. *SIAM Journal of Scientific Computing*, 23(1):339–361, 2001.
- [9] Z. Li, T. Lin, and X. Wu. New cartesian grid methods for interface problems using finite element formulation. *Numerische Mathematik*, 96:61–98, 2003.
- [10] X. Liu, R. P. Fedkiw, and M. Kang. A boundary condition capturing method for poisson’s equation on irregular domains. *Journal of Computational Physics*, 160(1):151–178, 2000.
- [11] X.-D. Liu and T. C. Sideris. Convergence of the ghost fluid method for elliptic equations with interfaces. *Mathematics of Computation*, 72(244):1731–1746, 2003.
- [12] A. Mayo. The Fast Solution of Poisson’s and the Biharmonic Equation on Irregular Regions. *SIAM Journal on Numerical Analysis*, 21(2):285–299, 1984.
- [13] A. Mayo. Fast high order accurate solutions of Laplace’s equation on irregular domains. *SIAM Journal Sci. Stat. Comput.*, 6(1):144–157, 1985.
- [14] M. Oevermann, R. Klein, M. Berger, and J. Goodman. A projection method for two-phase incompressible flow with surface tension and sharp interface resolution. Technical Report 00-17, Konrad-Zuse-Zentrum für Informationstechnik Berlin, May 2000.
- [15] C. S. Peskin. Numerical analysis of blood flow in the heart. *Journal of Computational Physics*, 25:220–252, 1977.
- [16] E. Süli. Convergence of finite volume schemes for poisson’s equation on nonuniform meshes. *SIAM Journal on Numerical Analysis*, 28(5):1419–1430, 1991.
- [17] S. Vater. A new projection method for the zero froude number shallow water equations. Technical Report 97, Potsdam Institute for Climate Impact Research, 2005.

## A Appendix

In section 3.4.1, equation (22), we introduced the matrices  $\underline{\underline{B}}_1$  and  $\underline{\underline{B}}_2$  to write  $\underline{b}^{(1)}$  in terms of  $\underline{x}^{(0)}$  and  $\underline{b}$ . The are given in detail here:

$$\underline{\underline{B}}_1 = (-1) \begin{bmatrix} 0 & \dots & \dots & \dots & \dots & 0 \\ \vdots & & & \ddots & & \vdots \\ 0 & \dots & \dots & \dots & \dots & 0 \\ \frac{1}{\varepsilon} & \frac{1}{\varepsilon} & \frac{a}{\varepsilon} & & \frac{a}{\varepsilon} & -\frac{1}{\varepsilon} & 0 & 0 & 0 \\ \frac{1}{\varepsilon} & \frac{b}{\varepsilon} & \frac{-1}{\varepsilon} & & \frac{b}{\varepsilon} & -\frac{1}{\varepsilon} & 0 & 0 & 0 \\ \frac{1}{\varepsilon} & \frac{1+b}{2\varepsilon} & \frac{1+a}{2\varepsilon} & & \frac{(1+a)(1+b)}{4\varepsilon} & -\frac{1}{\varepsilon} & 0 & 0 & 0 \\ 0 & \frac{\beta^{2\alpha} n_\xi}{\Delta x} & \frac{\beta^{2\alpha} n_\eta}{\Delta y} & \frac{\beta^{2\alpha} n_\xi(1+a)}{2\Delta x} & + \frac{\beta^{2\alpha} n_\eta(1+b)}{2\Delta y} & 0 & 0 & 0 & 0 \end{bmatrix}$$

and

$$\underline{\underline{B}}_2 = \begin{bmatrix} 0 & \dots & \dots & \dots & 0 \\ \vdots & & & \ddots & \vdots \\ 0 & \dots & \dots & \dots & 0 \\ 0 & \dots & 0 & \frac{1}{\varepsilon} & 0 & 0 & 0 \\ \vdots & \ddots & \vdots & 0 & \frac{1}{\varepsilon} & \vdots & \vdots \\ & & & \frac{1}{2\varepsilon} & \frac{1}{2\varepsilon} & & \\ 0 & 0 & 0 & \dots & 0 & \frac{1}{2} & \frac{1}{2} \end{bmatrix}.$$

## B Appendix

In section 3.4.2, equation (30), we introduced the matrices  $\underline{\underline{B}}_1$  and  $\underline{\underline{B}}_2$  to write  $\underline{b}^{(1)}$  in terms of  $\underline{x}^{(0)}$  and  $\underline{b}$ . The are given in detail here:

$$\underline{\underline{B}}_1 = \left[ \begin{array}{cccc|cccc} 0 & \dots & \dots & \dots & & & & 0 \\ \vdots & & & \ddots & & & & \vdots \\ 0 & \dots & \dots & \dots & & & & 0 \\ -1 & -a & 0 & 0 & 1 & \tilde{a} & 1 & \tilde{a} \\ -1 & -b & -1 & -b & 1 & \tilde{b} & 0 & 0 \\ 0 & 0 & 0 & -\frac{1}{4} & 0 & 0 & 0 & \frac{1}{4} \\ 0 & \frac{-\beta^{2\alpha} n_\xi}{\Delta x} & \frac{-\beta^{2\alpha} n_\eta}{\Delta y} & \frac{-\beta^{2\alpha} n_\xi}{2\Delta x} - \frac{\beta^{2\alpha} n_\eta(a+b)}{2\Delta y} & 0 & \frac{-\beta^{2\alpha} n_\xi}{\Delta x} & \frac{-\beta^{2\alpha} n_\eta}{\Delta y} & \frac{-\beta^{2\alpha} n_\xi}{2\Delta x} - \frac{\beta^{2\alpha} n_\eta(\tilde{a}+\tilde{b})}{2\Delta y} \end{array} \right]$$

and

$$\underline{\underline{B}}_2 = \begin{bmatrix} 0 & \dots\dots\dots & 0 \\ \vdots & & \ddots & & \vdots \\ 0 & \dots\dots\dots & 0 \\ 0 & \dots & 0 & 1 & 0 & 0 & 0 \\ \vdots & \ddots & \vdots & 0 & 1 & \vdots & \vdots \\ & & & 0 & 0 & 0 & 0 \\ 0 & \dots & 0 & 0 & 0 & \frac{1}{2} & \frac{1}{2} \end{bmatrix} .$$